CHEMMEDCHEM

DOI: 10.1002/cmdc.200700232

Synthesis, Biological Evaluation, and Molecular Modeling Studies of Rebeccamycin Analogues Modified in the Carbohydrate Moiety

Fabio Animati,[a] Marco Berettoni,[a] Mario Bigioni,[b] Monica Binaschi,[b] Patrizia Felicetti,[a] Lorenzo Gontrani,[d] Ottaviano Incani,[d] Andrea Madami,[c] Edith Monteagudo,[a] Lauso Olivieri,[a] Stefano Resta,[a] Cristina Rossi,[a] and Amalia Cipollone*[a]

A new series of indolocarbazole glycosides containing disaccharides were synthesized and their in vitro antiproliferative activity was evaluated against three human cancer cell lines (A2780, H460, and GLC4). Cytotoxicity appeared to be remarkably affected by the regio- and stereochemical features of the disaccharide moiety. In vivo antitumor activity of the compounds studied, two of which having $IC_{50} < 100$ nM, was determined using ovarian cancer cell line A2780 xenografted on nude mice. One compound showed an efficacy similar to that of the reference compound edotecarin, though with a lower long-lasting activity. The topoisomerase I inhibitory properties of some compounds were also examined. Molecular dynamics simulations of the ternary topoisomerase I–DNA–ligand complexes were performed to analyze the structural features of topoisomerase I poisoning with this class of indolocarbazoles. A plausible explanation of their biological behavior was provided. These theoretical results were compared with the recently published crystal structure of an indolocarbazole monosaccharide bound to the covalent human topoisomerase I–DNA complex.

Introduction

Indolocarbazole alkaloids constitute a group of natural compounds that have attracted attention as potential anticancer agents. The protein kinase C inhibitor, staurosporine, and the tumor growth inhibitor rebeccamycin (Figure 1), are representative members of this family.[1] The anticancer activity of rebeccamycin, which bears a glucose residue linked to a nitrogen atom of the indolocarbazole chromophore, has to be mainly ascribed to the inhibition of the catalytic cycle of topoisomerase I (top1), a nuclear enzyme involved in resolution of topological problems arising during DNA replication, transcription and recombination.[2] Top1 works by forming an intermediate covalent enzyme–DNA complex[3] through transesterification of the enzyme catalytic Tyr723 and the DNA 3′-phosphate at the cleavage site. This transient break allows the broken (scissile) DNA strand to rotate around the intact strand, removing superhelical tension.[4,5] Glycosylated indolocarbazoles of the rebeccamycin family were found to both intercalate into DNA and to stabilize the top1–DNA cleavable complex, preventing DNA re-ligation and thereby producing DNA lesions.[6]

Since the isolation of rebeccamycin, a considerable amount of research has been carried out to elucidate structure–activity relationships and to synthesize analogues with better pharmacological properties.[7–14] Indolocarbazole derivatives such as edotecarin[15] and BMS-250749 (Figure 1),[16] have entered clinical trials for the treatment of solid tumors.

The influence of chemical modifications of rebeccamycin on its biological activity has recently been reviewed.[17–19] The structural changes include all components of the glycosylated indolocarbazole structure, that is, the imide heterocycle, the planar chromophore, and the sugar residue. All the experimental observations agree in that the sugar moiety plays a crucial role: its removal leads to compounds completely devoid of activity; compounds possessing an α-*N*-glycosidic bond instead of the natural β bond do not behave as intercalating agents and have much less effect on top1. The replacement of glucose with other common pyranosides and furanosides does not result in any significant modification of top1 inhibition and cytotoxicity,[14] whereas the introduction of amino sugars[9] or partially hydroxylated sugars[7] produces more notable effects, depending on the substitution pattern.

[a] *Dr. F. Animati, Dr. M. Berettoni, Dr. P. Felicetti, Dr. E. Monteagudo, Dr. L. Olivieri, Dr. S. Resta, Dr. C. Rossi, Dr. A. Cipollone*
Chemistry Department, Menarini Ricerche S.p.A.
via Tito Speri 10, 00040 Pomezia Roma (Italy)
Fax: (+39) 06-9106137
E-mail: acipollone@menarini-ricerche.it

[b] *Dr. M. Bigioni, Dr. M. Binaschi*
Pharmacology Department, Menarini Ricerche S.p.A
via Tito Speri 10, 00040 Pomezia Roma (Italy)

[c] *Dr. A. Madami*
Molecular Modeling Department, Menarini Ricerche S.p.A
via Tito Speri 10, 00040 Pomezia Roma (Italy)

[d] *Dr. L. Gontrani, Dr. O. Incani*
Tecnofarmaci, via del Mare, 87–00040 Pomezia Roma (Italy)
and
C4T, Combinatorial Chemistry Center for Technology
Via della Ricerca Scientifica, 00143 Roma (Italy)

Supporting information for this article is available on the WWW under http://www.chemmedchem.org or from the author.

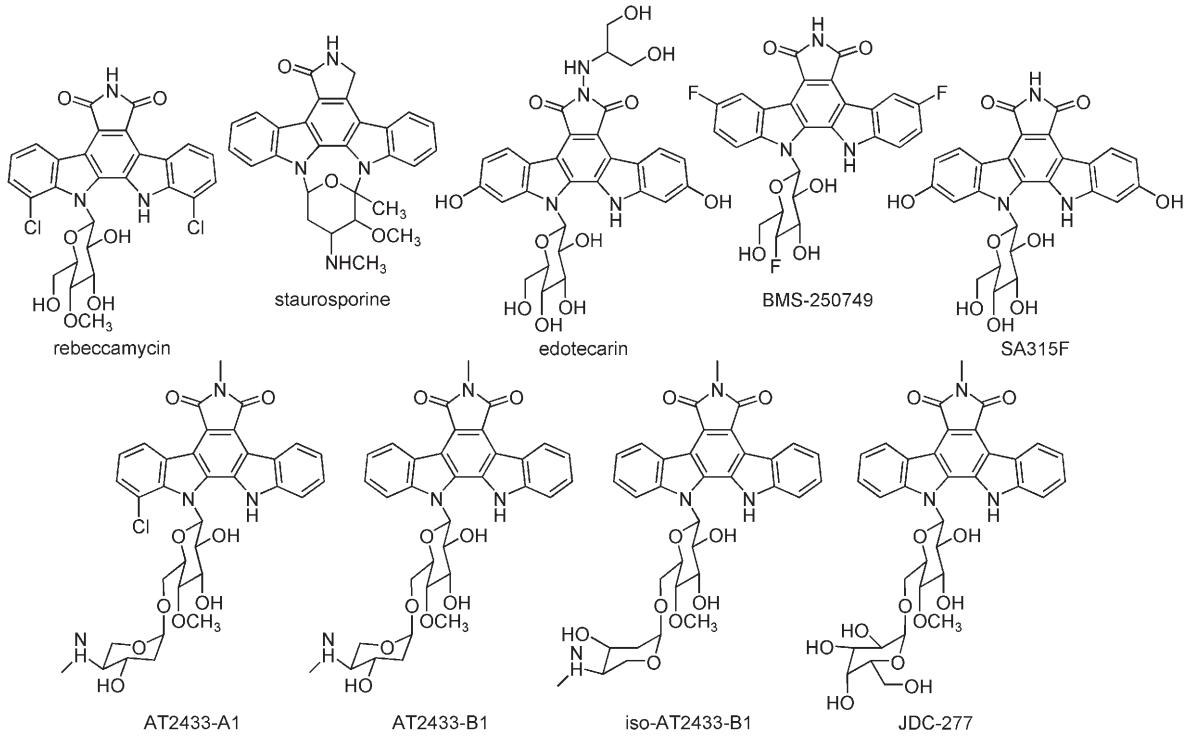

Figure 1. Structures of some mono- and diglycoside indolocarbazoles. Rebeccamycin, staurosporine, AT2433-A1, and AT2433-B1 are natural compounds; edotecarin and BMS-250749 are synthetic indolocarbazoles in clinical trials; SA315F is the indolocarbazole bound to the top1–DNA complex in the published X-ray crystal structure.[26]

Similar to other antitumor antibiotics substituted with carbohydrates, such as anthracyclines, calicheamicin, mithramycin, and bleomycin, the sugar moiety of rebeccamycin was thought to be positioned in one of the two helical grooves of DNA,[6] and attempts to increase interactions with DNA through introduction of a 2′-amino group[20] and of various halogenated acetyl groups[21] in the sugar moiety were reported. Taking into account the structural similarities between anthracyclines and indolocarbazoles, and the fact that elongation of the sugar moiety has led to an anthracycline currently in phase II clinical trials,[22] we postulated that the introduction of a second sugar residue onto the indolocarbazole core could improve the interactions in DNA grooves. To verify this hypothesis and to increase structure–activity relationship data of this class of compounds, a series of novel disaccharide indolocarbazoles were synthesized and studied (Figure 2).

To the best of our knowledge, few indolocarbazole disaccharides, either natural or synthesized, have been reported (Figure 1). AT2433-A1 and its dechlorinated derivative AT2433-B1, which bear an amino sugar as the terminal residue in the disaccharide, are highly cytotoxic in the human leukemia cell line CEM 2 as a consequence of their tight intercalative binding to DNA, preferentially to GC-rich sequences, while iso-AT2433-B1 is 20-fold less cytotoxic than its diastereomer. Interestingly, these compounds have no inhibitory effect on top1 in contrast to the uncharged diglycoside JDC-277, which stimulates DNA cleavage at TG sites as observed with camptothecin.[23–25] All these results indicate that the diglycosidic portion represents the primary structural determinant for DNA binding and sequence selectivity of these compounds.

To gain insight on structural determinants of the biological activity of this class of indolocarbazoles, molecular dynamics (MD) simulations were performed on some of the new compounds using the crystal structure of human top1 covalently bound to DNA[26] as the target for our flexible docking. Simulations of the ternary complexes were preceded by computational and NMR analysis of two isolated ligands. Shortly after conclusion of our work, the X-ray crystal structure of the indolocarbazole monosaccharide SA315F (Figure 1) bound to a top1–DNA complex was published,[27] and a comparison between this crystal structure and the results obtained by our MD simulations for the ternary top1–DNA–indolocarbazole disaccharide complexes was carried out.

Results and Discussion

Chemistry

Disaccharides were synthesized with the aim of varying regio- and stereochemical features such as configuration of the sugar components, orientation and position of the glycosidic linkage, and number of hydroxy groups in the sugar residues.

A convergent synthetic strategy was adopted to prepare compounds **1**–**13**: the aglycone and disaccharide moieties were synthesized separately and then linked to obtain the final glycosides. Disaccharides were obtained according to standard

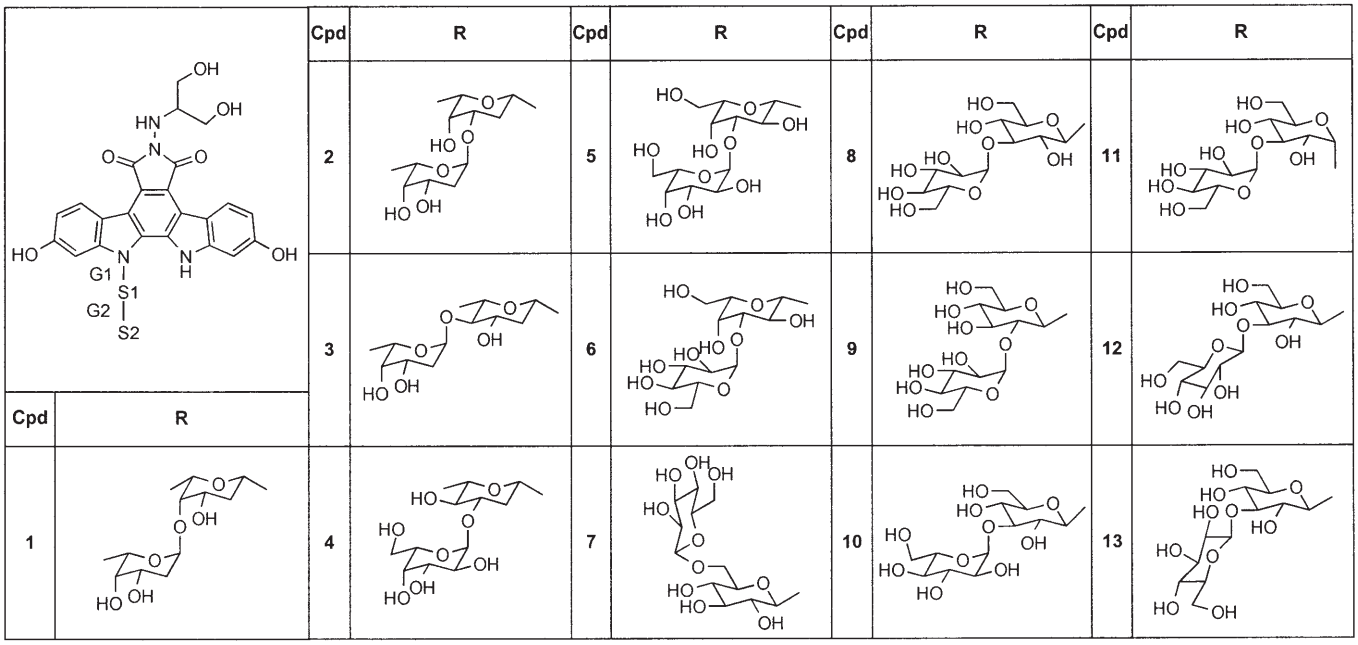

Figure 2. Structure of compounds **1**–**13**. G1 = glycosidic bond between aglycone and S1; S1 = sugar fragment linked to the aglycone; G2 = glycosidic bond between S1 and S2; S2 = second sugar fragment.

glycosylation protocols using phenyl thioglycosides or glycosyl chlorides as glycosyl donors, and *p*-methoxybenzyl or allyl glycosides as glycosyl acceptors. Both glycosyl donors and acceptors were synthesized from commercially available precursors.

Thioglycosides were adopted as glycosyl donors in the case of the 2-deoxy sugars owing to their enhanced stability relative to the corresponding glycosyl chlorides.[28] Glycosylation methodology is outlined in Scheme 1 for the preparation of 4-*O*-(3,4-di-*O*-benzyl-2-deoxy-α-L-fucosyl)-3-*O*-benzyl-2-deoxy-α-L-rhamnose **25**. Addition of *p*-methoxybenzyl alcohol[29] to the easily available 3,4-di-*O*-acetyl-L-fucal **14**,[30] followed by deacetylation with sodium methoxide, gave the *p*-methoxybenzyl fucoside **15**. Alkylation with excess benzyl chloride and potassium hydroxide as the base afforded *p*-methoxybenzyl-3,4-di-*O*-benzyl-2-deoxyfucoside **16**. Conversion of the anomeric *p*-methoxybenzyl group to the thiophenyl group was accomplished through deprotection with cerium(IV) ammonium nitrate,[31] reaction with *p*-nitrobenzoyl chloride to form the corresponding 1-*O*-*p*-nitrobenzoyl fucose **17**, followed by phenylthiotrimethylsilane and trimethylsilyl trifluoromethanesulfonate[32] to generate **18**. Direct conversion of the *p*-methoxybenzyl glycoside under the same reaction conditions was unsuccessful.

Synthesis of glycosyl acceptor **23** was achieved starting from 3,4-di-*O*-acetyl-L-rhamnal **19**,[30] which was submitted to exclusive *trans*-iodoalkoxylation with *p*-methoxybenzyl alcohol and *N*-iodosuccinimide,[33] followed by removal of iodine with tributyltin hydride[33] to give *p*-methoxybenzyl-3,4-di-*O*-acetyl-2-deoxyrhamnoside **21**. Deacetylation with sodium methoxide followed by alkylation with benzyl chloride and potassium hydroxide as the base gave a separable mixture of the two regioisomers **22** and **23** in a ratio of 3:2.

The two monomeric units **18** and **23** were coupled in the presence of freshly prepared iodonium dicollidine perchlorate (IDCP)[34] as iodonium source. This highly stereoselective glycosylation protocol provided disaccharide **24** almost exclusively with the desired α linkage.[35,36] Mild removal of the anomeric *p*-methoxybenzyl group with 2,3-dichloro-5,6-dicyanobenzoquinone[37] afforded the free disaccharide **25**.

The glycosylation procedure using glycosyl chlorides as glycosyl donors is illustrated in Scheme 2 for the preparation of 3-*O*-(2,3,4,6-tetra-*O*-benzyl-α-D-glucosyl)-2,4,6-tri-*O*-benzyl-α-D-glucose **34** and of the corresponding β isomer **35**. Commercially available tetra-*O*-benzyl-D-glucose **26** was quantitatively converted into the 1-chloro glycoside **27** with oxalyl chloride.

The glycosyl acceptor allyl-4,6-*O*-benzylidene-2-*O*-benzyl-D-glucoside **31** was obtained from D-glucose **28**. Protection of the anomeric position with allyl alcohol and a cationic resin, followed by selective protection of hydroxy groups in positions 4 and 6 as benzylidene acetal by treatment with benzaldehyde and zinc chloride, provided the allyl glycoside **29**.[38] Alkylation with benzyl chloride and potassium hydroxide as the base afforded **31** together with its regioisomer **30** (in a ratio of 1:4), easily separated by flash chromatography on silica gel.

Coupling of **31** with the glycosyl donor **27** in the presence of silver triflate as promoter[39] gave a separable mixture of the α and β isomers (compounds **32** and **33**, respectively, in a ratio of 7:3), due to less efficient control of stereochemistry in this glycosylation methodology relative to iodonium-mediated reactions. Deprotection of the benzylidene moiety with trifluoroacetic acid, benzylation of the free hydroxy groups with benzyl bromide, and mild removal of the anomeric allyl group with palladium chloride[40] afforded the corresponding free disaccharides **34** and **35**.

The synthetic sequence to obtain the final compounds **1**–**13** is represented in Scheme 3 for the glycoside **12**. Introduction of the disaccharides on the indolocarbazole core was per-

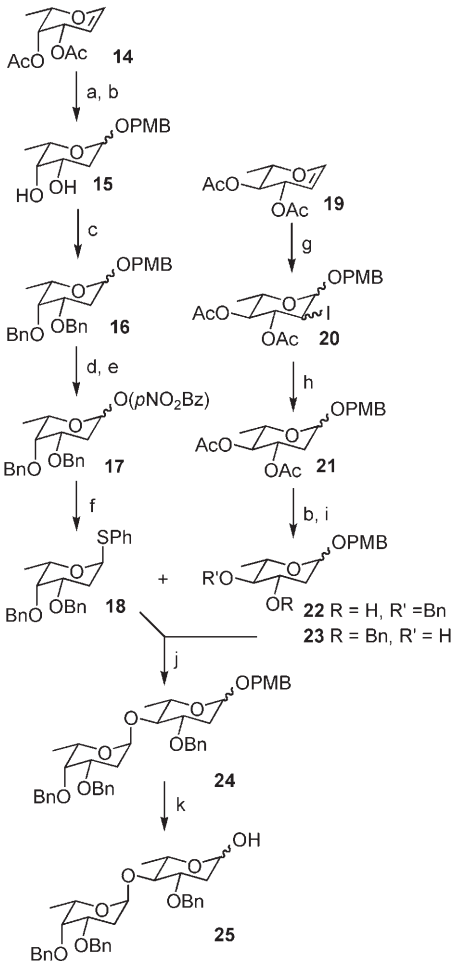

Scheme 1. Reagents and conditions: a) *p*-MeOBnOH (2 equiv), $(Ph)_3PHBr$ (0.05 equiv), CH_2Cl_2, 20 °C, 3 h, 60%; b) MeONa (0.3 equiv), MeOH, 0→20 °C, 1 h, quant.; c) BnCl (5 equiv), KOH, dioxane, reflux, 88%; d) $Ce(NH_4)_2(NO_3)_6$ (2 equiv), CH_3CN/H_2O (9:1), 20 °C, 3 h, 90%; e) *p*-NO_2BzCl (3 equiv), DMAP (0.1 equiv), pyridine (3 equiv), CH_2Cl_2, 20 °C, 82%; f) $PhSSi(Me)_3$ (4.5 equiv), $CF_3SO_3Si(Me)_3$ (2.5 equiv), CH_2Cl_2, 0→20 °C, 24 h, 88%; g) *p*-MeOBnOH (2 equiv), NIS (1.6 equiv), CH_3CN, 20 °C, 24 h, 90%; h) Bu_3SnH (1.4 equiv), AIBN (0.15 equiv), toluene, 80 °C, 4 h, 90%; i) BnCl (2 equiv), KOH, dioxane, 20 °C, 65%; j) IDCP (2 equiv), molecular sieves 4 Å, Et_2O/1,2-dichloroethane (4:1), 20 °C, 4 h, 90%; k) DDQ (1.4 equiv), CH_2Cl_2/H_2O (50:1), 20 °C, 30 min, 50%. AIBN = azobisisobutyronitrile, IDCP = iodonium dicollidine perchlorate, NIS = *N*-iodosuccinimide, PMB = *para*-methoxybenzyl.

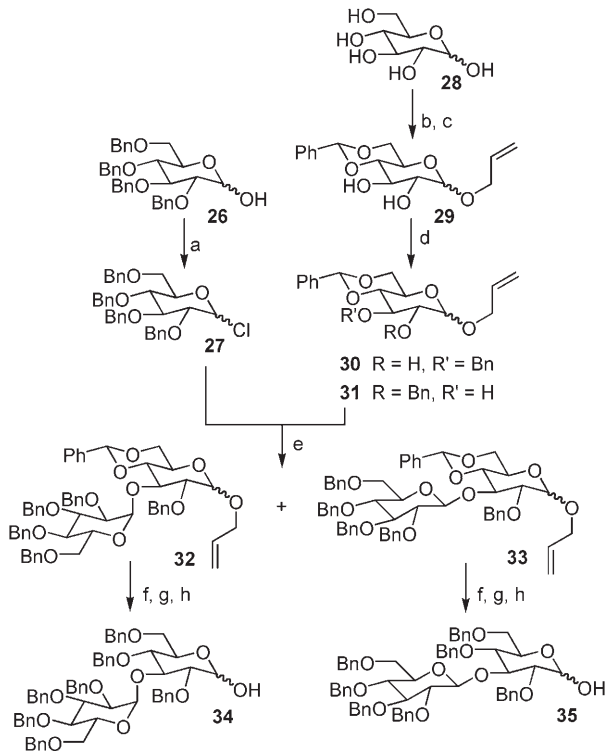

Scheme 2. Reagents and conditions: a) $(COCl)_2$ (2 equiv), CH_2Cl_2/DMF (cat.), 20 °C, 45 min, quant.; b) allyl alcohol, Amberlist 15, 100 °C, 3 h, 50%; c) PhCHO, $ZnCl_2$, 20 °C, 48 h, 70%; d) BnCl (1.2 equiv), KOH, dioxane, 100 °C, 1 h, 78%; e) AgOTf (1.2 equiv), sym-collidine (1.2 equiv), 2 h, 20 °C, 80%; f) TFA/CH_2Cl_2 (1:2), 0 °C, 2 h, 65%; g) BnBr, NaH, DMF, 0→20 °C, 2 h, 90%; h) $PdCl_2$ (1 equiv), MeOH, 20 °C, 3 h, quant.

formed according to the methodology developed by Okhubo,[41] in which a glycosyl chloride was treated with the anion of the indolocarbazole aglycone in heterogeneous basic media. Free sugar **35** was converted into glycosyl chloride **36** with oxalyl chloride and treated with the dianion of the aglycone **37**,[42] generated by powdered potassium hydroxide in acetonitrile to afford the desired β-glycoside **38** as the major isomer (ratio α/β = 0.2:9.8).

The same glycosylation methodology was applied to the other disaccharides, to obtain the corresponding indolocarbazole glycosides in yields ranging from 20 to 60%, with a prevalence of the β isomer (α/β ratio ranging from 1:16 to 3:7). After hydrogenolysis of the benzyl groups with 10% Pd/C, the imido function was converted into anhydride **39** by treatment with aqueous potassium hydroxide.[41] Coupling of the anhydride with the hydrazine **40**[43] in DMSO and at room temperature[43] afforded **12** in good yield.

Compounds **1**–**6** are characterized by the first sugar (S1) belonging to the L series (Figure 2): specifically, S1 is 2-deoxyfucose (in compounds **1**, **2**), its 4-epimer, 2-deoxyrhamnose (in compounds **3**, **4**) and galactose (in compounds **5**, **6**). For derivatives **7**–**13** S1 is D-glucose. To verify the influence of the G2 position on the biological activity of these compounds, a D-glucose residue (S2), was linked to positions 6, 3, and 2 of S1, affording the regioisomeric glycosides **7**, **8**, and **9**. As substitution at position 3 appeared to be most favorable for biological activity, we also introduced α-L-glucose (in compound **10**), β-D-glucose (in compound **12**), and β-L-glucose (in compound **13**) units in this position. For both series, the *N*-glycosidic linkage between the aglycone and the disaccharides (G1) is β, except for compound **11**.

Inhibition of topoisomerase I

Induction of DNA cleavage mediated by recombinant DNA top1 was analyzed in the presence of compounds **1** and **8** (Figure 3). Compound **1** appeared less potent in the stimulation of DNA cleavage than compound **8** and edotecarin. Both compounds showed a sequence specificity similar to that observed for edotecarin. Differences were instead observed re-

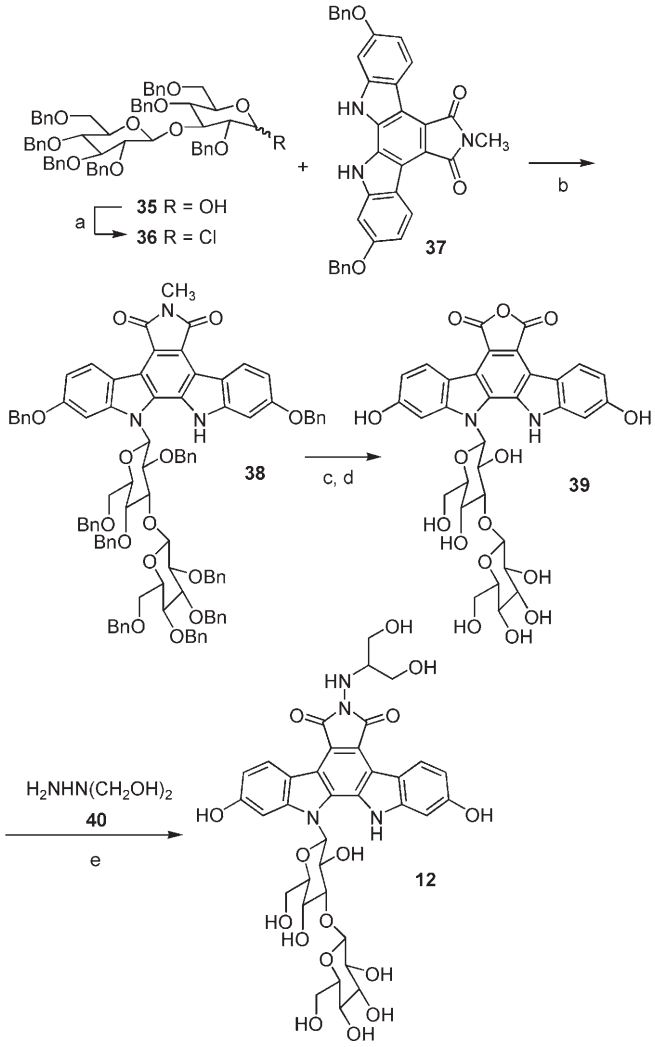

Scheme 3. Reagents and conditions: a) $(COCl)_2$ (2 equiv), CH_2Cl_2/DMF (10:1), 20 °C, 30 min; b) KOH (7 equiv), Na_2SO_4, CH_3CN, 20 °C, 1 h, then **36** (1 equiv) in CH_3CN, 10 h; c) 10% Pd/C, H_2, $CH_3OH/CHCl_3$ (1:1); d) 2 N KOH (55 equiv), 20 °C, 5 h; e) **40** (4 equiv), DMSO, 20 °C, 2 h.

garding the relative DNA cleavage intensities of the sites stimulated by derivative **8**.

Cytotoxicity

The in vitro antiproliferative activity of compounds **1**–**13** was determined against a panel of three human cancer cell lines, including ovarian cancer (A2780), lung cancer (H460) and small-cell lung cancer (GLC-4). Edotecarin and camptothecin were used as reference compounds (Table 1). The H460 cell line was weakly responsive to the tested compounds. In the A2780 and GLC4 cell lines, the new molecules showed similar cytotoxicity profiles, although some differences in potency were observed. In particular, compound **8** seemed the most active in both cancer cell lines.

Compounds **1**–**6** showed lower cytotoxicity in comparison with the reference compounds. Interestingly, regioisomers **1** and **2**, with the same 2-deoxyfucosyl-2-deoxyfucose moiety, exhibited very different cytotoxicities according to the G2 position: the 1,3 linkage in **2** (IC_{50}: 0.1 μM in A2780 and 0.021 μM in GLC4) seemed to be more favorable than the corresponding 1,4 linkage in **1** (IC_{50}: 79.9 μM in A2780 and >1 μM in GLC4). However, if S1 was changed from 2-deoxyfucose in **1** to its 4-epimer 2-deoxyrhamnose in **3** (IC_{50}: 0.32 μM and 0.2 μM in GLC4), the 1,4 linkage allowed a remarkable recovery of cytotoxicity. The introduction of α-L-galactose (S2) in position 3 of 2-deoxyrhamnose in **4** did not confer higher cytotoxicity. Simi-

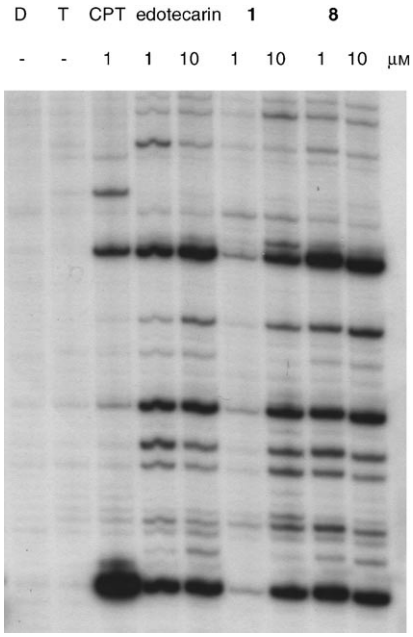

Figure 3. Top1-mediated cleavage of SV40 DNA fragment in the presence of camptothecin (CPT), edotecarin, and the indolocarbazoles **1** and **8**. Purified top1 was incubated with SV40 DNA fragment in the absence (lane T) or presence of the drugs at the indicated concentrations. Top1 cleavage reactions were performed as described in the Experimental Section and then analyzed in a denaturing 8% polyacrylamide gel. Lane D: DNA control sample.

Table 1. In vitro antiproliferative activities of compounds **1**–**13** against ovarian carcinoma (A2780), lung carcinoma (H460), and small-cell lung carcinoma (GLC4) cells.

Compd	IC_{50} [μM][a] A2780	H460	GLC4
1	79.9 ± 34.8	90.66 ± 16.1	>1
3	0.32 ± 0.098	>1	0.2 ± 0.06
4	>1	>1	0.255 ± 0.007
5	0.43 ± 0.065	>1.7	0.052 ± 0.0035
6	0.43 ± 0.049	>1	0.147 ± 0.01
7	0.51	>1	0.2
8	0.007 ± 0.001	1.8 ± 0.5	0.01 ± 0.002
9	4.3 ± 1	>7.5	1.45
10	0.27 ± 0.075	1.25 ± 0.15	0.02 ± 0.01
11	0.1	13.35 ± 0.7	0.035 ± 0.005
12	0.049 ± 0.013	>0.5	0.104 ± 0.04
13	0.21 ± 0.03	>0.25	0.35 ± 0.042
edotecarin	0.0065 ± 0.0004	0.193 ± 0.145	0.0008 ± 0.0001
CPT[b]	0.007 ± 0.006	0.005 ± 0.004	0.010 ± 0.008

[a] Values represent the mean ± SE of three independent determinations. [b] Camptothecin.

larly, substitution of both S1 and S2 with fully hydroxylated sugars did not seem to improve cytotoxicity (compounds **5** and **6** versus **2**) regardless of the second sugar belonging to the L or D series (**5** versus **6**).

Among the regioisomers **7**, **8**, and **9**, bearing a D-glucosyl-D-glucose the disaccharide moiety, an α-1,3 linkage between S1 and S2 in **8** was much more cytotoxic than the corresponding 1,2 linkage in **9** and the 1,6 linkage in **7** (600- and 70-fold in A2780, and 145- and 20-fold in GLC4, respectively), and showed the same activity as edotecarin in the A2780 cell line. Inversion of G2 configuration in **8** led to the β stereoisomer **12** with decreased cytotoxicity. In contrast, if S2 was changed to L-glucose, the resulting α and β isomers (**10** and **13**, respectively) were almost equally cytotoxic, and both displayed decreased activity with respect to the corresponding D analogues **8** and **12**.

Derivative **11**, with G1 in the α configuration, was less cytotoxic than the corresponding β isomer **8** (IC_{50} 0.1 μM in A2780 and 0.035 μM in GLC4 compared with IC_{50} 0.007 μM in A2780 and 0.01 μM in GLC4), confirming the preferred β configuration of the linkage between the aglycone and the carbohydrate residue.[18]

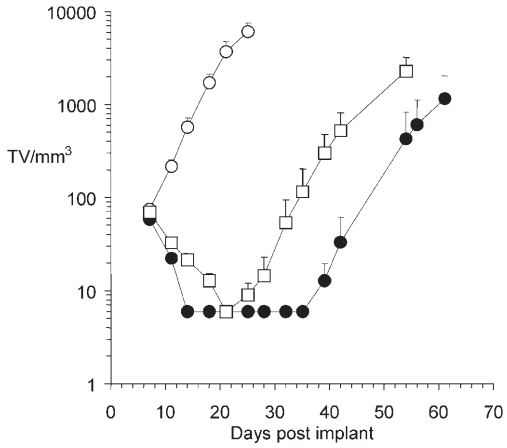

Figure 5. Antitumor activity of **12** (□, 120 mg kg^{-1}) on A2780 human ovarian carcinoma xenograft model. Edotecarin (●) was used as reference compound; negative control (○) is also indicated.

Antitumor activity

On the basis of their cytotoxic potency, compounds **8** and **12** were evaluated for their effects in inducing tumor regression in the A2780 human ovarian carcinoma xenograft model. The compounds were administered i.v. with a twice weekly schedule (q4d×4) at different doses, as illustrated in Figure 4 and Figure 5.

Compound **8**, at a dose of 50 mg kg^{-1}, showed an efficacy comparable to that of edotecarin in terms of tumor volume inhibition, although the long-lasting antitumor activity appeared to be lower, as indicated by a lower value of LCK (log cell kill; edotecarin: 4.0, **8**: 2.9; Table 2). At a higher dose (100 mg kg^{-1}) **8** was toxic for all mice treated. The β isomer **12**, at a dose of 120 mg kg^{-1}, exhibited antitumor activity comparable to compound **8**. No toxic effect was found at this schedule and dosage.

Table 2. Antitumor efficacy of compounds **8** and **12** on A2780 xenograft model.

Compd	Dose [mg kg^{-1}]	Schedule, Route	TVI [%][a]	LCK (1 g)[b]	Deaths/Total[c]
edotecarin	100	q4d×4, i.v.	99.4	4.0	1/4
8	25	q4d×4, i.v.	99.5	2.8	0/5
8	50	q4d×4, i.v.	99.4	2.9	1/5
edotecarin	90	q4d×4, i.v.	99.0	5.3	0/5
12	120	q4d×4, i.v.	99.0	4.0	0/5

[a] Tumor volume inhibition in treated versus control mice determined at the nadir of tumor volume in the treated group. [b] Log cell kill = T−C/DT×3.32, for which T and C represent the time (in days) taken by the tumors in treated (T) and control (C) mice to reach a predetermined volume specified in each experiment. DT is the tumor doubling time calculated from semilogarithmic best-fit curve of tumor volume in the control group plotted versus time when the growth of tumor was in the exponential phase. [c] Number of deaths out of the total number of mice.

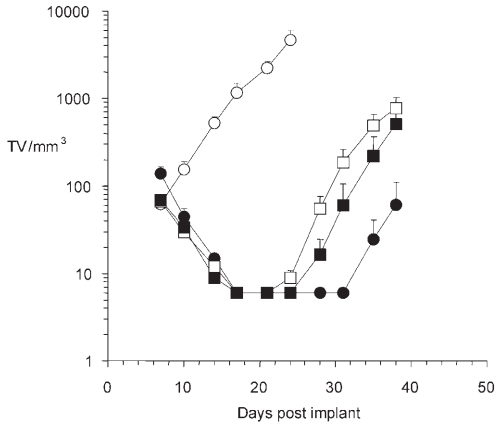

Figure 4. Antitumor activity of **8** at 25 (□) and 50 (■) mg kg^{-1} on A2780 human ovarian carcinoma xenograft model. Edotecarin (●) was used as reference compound; negative control (○) is also indicated.

Conformational analysis of indolocarbazoles

MD simulations of the ternary complexes were preceded by NMR and computational analysis of two selected ligands (**1** and **2**). The purpose of these preliminary studies was to test the reliability of computational methods in reproducing the conformational preferences of our molecules.

Conformations of the glycosidic linkage G1 were studied through NOESY experiments.[44] For compound **1** two medium NOE cross peaks were measured between H1′ of S1 and H1 of the aglycone, and between H1′ and NH12, thus showing that the two conformers called iso1 and iso2 had similar probability (Figure 6). In contrast, for compound **2**, a single strong NOE signal between H1′ and H1 was detected, indicating that in this case, conformation iso1 was predominant.

MD simulations, with explicit solvent, of the two indolocarbazoles were performed with the AMBER[45] force field extend-

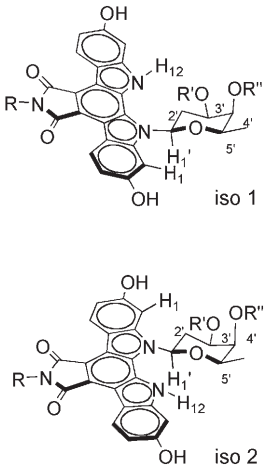

Figure 6. Structures of the two conformations iso1 and iso2 for compounds **1** [R = $NH(CH_2OH)_2$; R′ = H; R″ = 2-deoxy-α-L-fucose] and **2** [R = $NH(CH_2OH)_2$; R′ = 2-deoxy-α-L-fucose; R″ = H].

ed to carbohydrates as reported previously,[46] and improved with new parameters for indolocarbazoles, as described in the Experimental Section below. For compound **1**, the two conformers, iso1 and iso2, were found to have almost the same energy, whereas for compound **2**, iso1 resulted to be about 6 kcal mol^{-1} more stable than iso2. The agreement between MD results and experimental findings indicates that the force field has been satisfactorily extended to indolocarbazoles and is therefore suitable for MD simulations of the ternary complex.

Molecular dynamics study of the ternary complex

The X-ray crystal structure of human top1 covalently bound to DNA[26] was used to study, by MD, the behavior of **1**, **2**, **4**, **8**, **9**, and **12** in the ternary top1–DNA–indolocarbazole complexes. Compounds were selected as representatives of both the L (in **1**, **2**, and **4**) and D (in **8**, **9**, and **12**) series and were endowed with a biological activity ranging from the inactive compounds **1** and **9** to the active compounds **2**, **8**, and **12**. On the basis of the crystallographic structure and of a series of chemical and biochemical observations, Redinbo and co-workers[26] proposed a hypothetical binding region for the natural top1 poison camptothecin into the top1–DNA complex, constituted by five key residues: Arg 364, Asp 533, Asn 722, the guanine base flanking the cleavage site on the 3′ side of the scissile strand (G + 1s), and C + 1s. Taking into account the similarity[47] between camptothecins and indolocarbazoles in the interaction with the cleavable complex, we selected these residues as the putative binding site for the indolocarbazoles in the binary top1–DNA complex.

The initial position of the ligand in the binding region was defined using compound **1** as a model and was subsequently employed in MD simulations of the ternary complexes for all the other compounds. Indolocarbazole **1**, placed far from the biomolecules, was docked using constrained MD into the binding site of the covalent top1–DNA complex. Eight docking simulations were performed to ensure a significant exploration of the conformational space. Four of them started from **1** (iso1) and four from **1** (iso2), to avoid any possible bias towards one conformer with respect to the other. A large region of the biomolecular system was free to move in MD processes, thus allowing the binary complex to receive the indolocarbazole and to rearrange in the optimal way during docking. The constraint, used to force the docking, was removed in the final period of MD to verify the permanence of **1** in the hypothetical binding region. After optimization of the top1–DNA–**1** structures sampled during simulation, the disaccharide residue of **1** in the most stable complex was replaced by those of the other ligands (**2**, **4**, **8**, **9**, and **12**.) The six top1–DNA–indolocarbazole complexes obtained were finally submitted to an extended and unconstrained MD simulation (Figure 7).

These simulations were analyzed by evaluating the solvent-accessible surface (SAS) and buried surface (BS) for the aglycone and the disaccharide (Table 3 and Table 4). All the indolocarbazoles show similar results for the aglycone moiety for which SAS values fall in the range of 15 to 25% of the total surface, and BS amounts indicate that comparable interactions

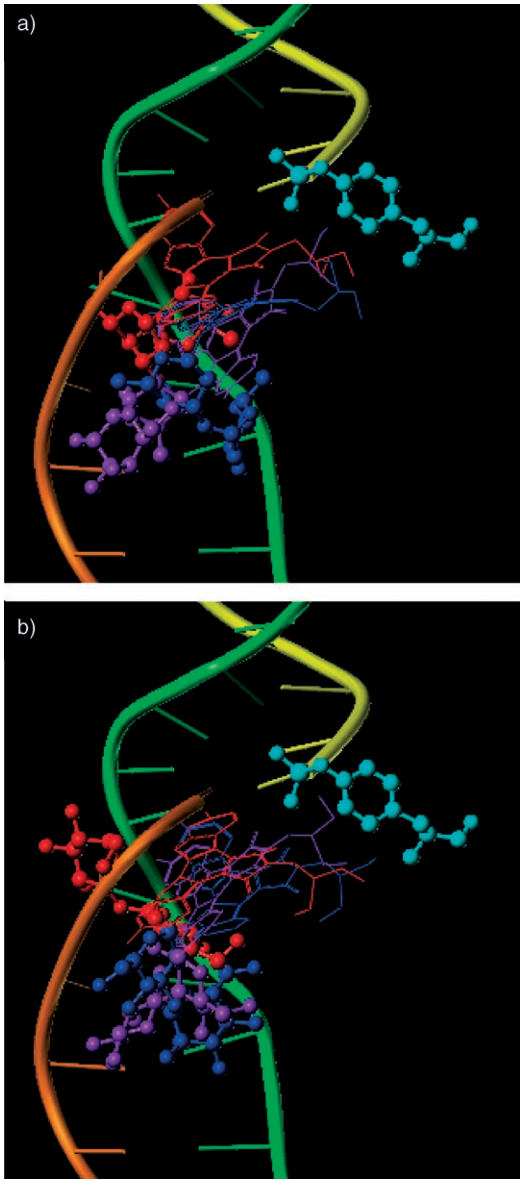

Figure 7. Schematic representations of the top1–DNA–indolocarbazole complexes. DNA is displayed as tubes, the intact strand in green, the scissile strand in yellow (5′ side) and orange (3′ side). Heavy atoms of the phosphotyrosine 723 residue are in cyan. The aglycone and the disaccharides of the indolocarbazoles are displayed as lines, balls, and sticks, respectively. a) Partially dehydroxylated indolocarbazoles: **1** (red), **2** (blue), and **4** (violet). b) Fully hydroxylated indolocarbazoles: **8** (blue), **9** (red), and **12** (violet). The structures were obtained from the clustering of the MD trajectories as described in the Experimental Section (**2** and **8** each had two representative structures; for clarity, only one of them is shown).

Table 3. Solvent-accessible surface (SAS) and buried surface (BS) for the aglycone and disaccharide fragments evaluated on the representative structures obtained in the MD simulations.

Compd	Aglycone		Disaccharide	
	SAS	BS	SAS	BS
1	68	286	14	212
2[a]	88	282	100	162
4	59	312	83	162
8[a]	96	281	75	197
9	85	281	12	252
12	79	293	61	225

[a] SAS and BS values (in Å^2) of **2** and **8** are the average of the values obtained for two representative structures.

with the residues of the macromolecular system are present. Among them the most relevant (higher BS values) is a π–π stacking interaction with G+1s.

Conversely, SAS and BS parameters for the disaccharide moiety show a larger range of values. The SAS for **1** and **9**, to which we refer as inactive compounds (Table 1), is about 5% of the whole surface, whereas the active molecules (**2**, **8**, and **12**) and compound **4**, endowed with an intermediate activity among the six compounds studied, expose to solvent between 20 and 40% of the total surface. Moreover, BS values indicate that while all disaccharides interact with A+3s, only active molecules (**2**, **8**, and **12**) and **4** are able to stretch towards DNA bases A+4s, T+5i, A+5s and T+6i, far from the cleavage site. Compounds **1** and **9**, in contrast, tend to bend towards G+1s, C+1i, A−1i and A−2i, which are near the DNA break.

MD trajectories were then studied by measuring the intermolecular distances (see Supporting Information) between indolocarbazoles and biomolecules. This analysis points out that compounds **2**, **8**, and **12** make hydrogen bonds with bases A+4s, T+5i and A+5s, unlike the inactive compounds (**1** and **9**) and **4**. Compounds **1** and **2** bear the same 2-deoxyfucosyl-2-deoxyfucose group as disaccharide moiety, but in the former, the glycosidic bond G2 in position 4′ allows an H bond S1–S2, between OH3′ and O5″, while in the latter this bond cannot be formed, because G2 is in position 3′, and there are no H-bond donor or acceptor groups at a suitable distance (Figure 8). This behavior can explain the greater conformational mobility of **2** with respect to **1**. Compound **4** has G2 in position 3′ like **2**, but the conformational mobility is limited because the H bond linking OH6″ of S2 and the hydroxy group of the indole ring bearing the disaccharide moiety. For indolocarbazoles **8**, **9**, and **12**, having both S1 and S2 fully hydroxylated, intramolecular H bonding S1–S2 is facilitated with respect to **1**, **2**, and **4**. Nevertheless, differences were observed within this set of compounds. For instance, in **9** the S1–S2 H bond is formed by OH2″ of S2, whereas in **8** the bond is formed by O5″.

Therefore, in compound **8**, the H-bond donor/acceptor group OH2″ is available for interaction with the biomolecular system, while in **9** this contact is substituted by the less powerful H-bond acceptor O5″. Moreover, as observed for **1** and **2**, also for **8**, **9**, and **12**, the G2 position appears to be the critical factor in determining different conformational mobilities. In **9** G2 is in position 2′ of S1, so that S2 is spatially near to the aglycone and an H bond exists between O5″ and NH of the indole ring. Indolocarbazoles **8** and **12** have G2 in position 3′, and the NH group of the indole forms an H bond with OH2′,

Table 4. Analysis of the ligand surface buried by each residue of the biomolecular system evaluated for representative structures resulting from MD simulations.[a]

Residue[b]	**1**	**2**[d]	**4**	**8**[d]	**9**	**12**
Arg 364					●	
Asp 533					●	
Lys 720	○○○●●●	○○○○	○○○	○○○○○●●●	○○○○●●●●	○○○●●●
Leu 721	○	○	○○○○	○○	○	○○
Asn 722	○○	○○	○	○○○○		○
P-Tyr 723[c]	○○	○	○○○		○○○	○○○
T+6i		●●	●			
A+5s		●●	●●●●	●●		●●
T+5i		●●	●			●●
A+4s		●●●●●	●●	●●		●●
T+4i	○●●●	○	●●●	●●		●●●
A+3s	○●●●●●●	○○●●●●●		○●●●●●●●	○○●●●●●	○●●●●●●●●
T+3i	●●	○	●●	●●	●	●●
G+2s	○○○○●●●	○○○○○●	○○○●●●●	○○○○○●●	○○●●●●	○○○○●
C+2i	●●	○			●	●●
G+1s	○○○○○○○	○○○○○○○○	○○○○○○	○○○○○○○	○○○○○○○●●	○○○○○○
G+1i	○●●	○			●	○○
T−1s	○○	○○	○○○○	○○○○	○○○	○○○○
A−1i					●●●	
T−2s					○	
A−2i	○○		○	○○	○○●	○○

[a] ○ and ● represent 5 Å^2 of the surface of the aglycone and disaccharide, respectively. [b] Only residues that bury at least 5 Å^2 of the surface of the aglycone or disaccharide are reported. [c] P-Tyr: phosphotyrosine residue. [d] BS value of **2** and **8** are the average of the values obtained for two representative structures.

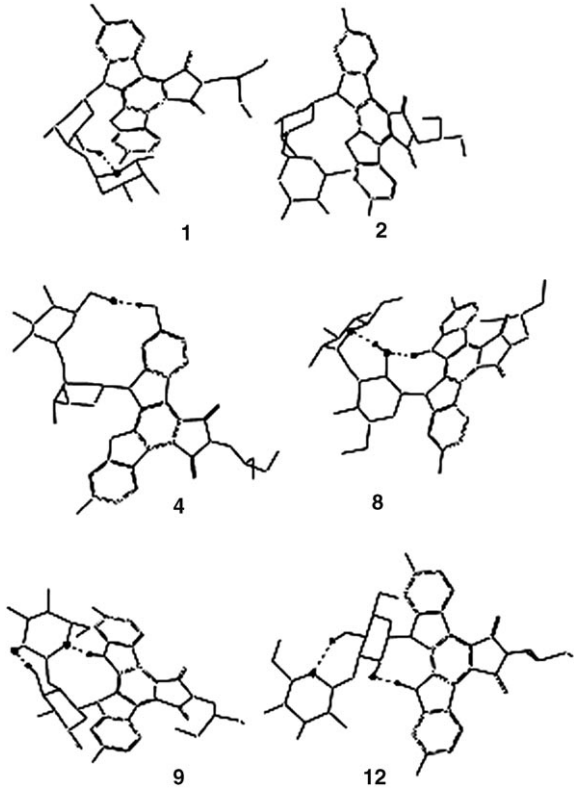

Figure 8. Indolocarbazole intramolecular H-bond interactions in representative structures obtained in MD simulations of the ternary top1–DNA–indolocarbazole complexes (**1**, **2**, **4**, **8**, **9**, **12**). Hydrogen bonds are shown with dashed lines.

while S2 can arrange itself distant from the aglycone, and is thus able to interact with bases far from the cleavage site.

Comparison with crystallographic results

A superposition of the X-ray crystal structure of the top1–DNA–SA315F complex (PDB code: 1SEU) and the X-ray crystal structure (PDB code: 1A31) of the binary top1–DNA complex used in our MD simulations, reveals good similarity (root-mean-square deviation (RMSD) 0.8 Å) except for the active site region, where the intercalating ligand pulls the surrounding DNA bases apart. The distances between T−1s and G+1s and between A−1i and C+1i are approximately doubled so that the ligand intercalates at the typical stacking distance of 3.5 Å. Comparison of 1SEU with the complexes between 1A31 and **1**, **2**, **4**, **8**, **9**, and **12** obtained by MD shows RMSD values for the biomolecular residues in the range 1.5–1.6 Å, with the most relevant differences found in the active site. This is not a surprising result, taking into account that the X-ray structure depicts the final "frozen" geometry of the binding process, whereas our unrestrained MD describe "hot" situations, when the ligand binding and the related complex rearrangement of the active site are occurring.

The X-ray structure of the top1–DNA–SA315F gave us the opportunity to try a high-throughput docking method in which biomolecules are kept rigid, to study the binding of **1**, **2**, **4**, **8**, **9**, and **12**. These indolocarbazoles and, for comparison, SA315F were docked into the biomolecular system of 1SEU using the program GOLD.[48] Both for SA315F and for indolocarbazole disaccharides, the majority of the docking solutions were placed in the active site; furthermore, the best-scored pose of SA315F was in acceptable agreement with the crystallographic structure (RMSD: 1.0 Å). Compared with SA315F, all the indolocarbazole disaccharides have a lesser tendency to give intercalative structures, almost certainly due to the increased steric hindrance of the second sugar and of the substituent on the imide heterocycle nitrogen atom. Analysis of the score and geometry of the docking poses of **1**, **2**, **4**, **8**, **9**, and **12** into 1SEU did not permit semi-quantitative or qualitative correlations with the biological activity of the compounds.

Conclusions

A series of rebeccamycin analogues bearing structurally different disaccharides have been investigated. The regio- and stereochemical features of the sugar residues appeared to determine the biological activity of this class of potential anticancer agents. Molecular modeling studies provided a plausible explanation for this behavior. MD simulations indicated that while the more active molecules (**2**, **8**, and **12**) are able to reach DNA bases A+4s, T+5i, and A+5s far from the cleavage site and to form hydrogen bonds with them, compound **4**, with decreased activity, is not able to form such a hydrogen bond network, although reaching these bases, and the less active molecules (**1** and **9**) tend to bend towards bases G+1s, C+1i, A−1i, and A−2i, which are near to the DNA break. These findings, caused by a diverse pattern of intramolecular H-bonding interactions, could be exploited to design sugar moieties able to more effectively stabilize the top1–DNA cleavable complex.

Experimental Section

General methods

Commercially available chemicals and solvents were reagent grade and used without further purification. All moisture-sensitive reactions were performed under a nitrogen atmosphere, using anhydrous solvents. Starting materials were dried by azeotropic evaporations with anhydrous toluene. Molecular sieves (4 Å) were activated by heating under reduced pressure. Merck silica gel (Kieselgel 60) was used for analytical thin-layer chromatography (TLC, F_{254} plates) and flash chromatography (40–63 μm). Purity was determined by HPLC using a 600 E Waters pump coupled to a Jasco 875 UV detector and a Merck–Hitachi D-2500 integrator. The HPLC column was Merck LiChrospher (RP-18, 5 μm, 250×4 mm), and the solvents were water with 0.1% trifluoroacetic acid (A) and acetonitrile with 0.1% trifluoroacetic acid (B). A linear gradient was used from 60 to 40% A over 30 min at a flow rate of 1 mL s^{-1} and UV detection at 220 nm.

^{1}H NMR and ^{13}C NMR experiments were recorded on a Varian Gemini 300 MHz or on a Bruker Avance 400 MHz spectrometer at 25 °C. Chemical shifts are reported in δ units (ppm) and are referenced to residual solvent signal: [D_6]DMSO (δ = 2.49 ppm). They are assigned as singlets (s), doublets (d), doublets of doublets (dd),

triplets (t), quartets (q), quintets (quin), multiplets (m), and broad signals (br).

General glycosylation procedure

Oxalyl chloride (0.46 mmol) was added dropwise to a solution of the free disaccharide (0.23 mmol) in anhydrous CH_2Cl_2 (14 mL) and anhydrous DMF (1.4 mL). After completion of the reaction (30 min), solvent was removed under reduced pressure and the residue evaporated twice with toluene. In the meantime, 5*H*-indolo[2,3-*a*]pyrrolo[3,4-*c*]carbazole-12,13-dihydroxy-2,10-dibenzyloxy-6-methyl-5,7(6*H*)-dione **37** (0.23 mmol) was added to a suspension of finely powdered KOH (1.62 mmol) and Na_2SO_4 (1.70 mmol) in dry CH_3CN (14.4 mL) under nitrogen atmosphere. The resulting dark-purple suspension was stirred for 30 min and then a solution of the 1-chloro disaccharide in dry CH_3CN (16 mL) was added over 10 min. After 24 h at 50 °C, the mixture was poured into ice/water (200 mL), neutralized with 1 N HCl and extracted with EtOAc (150 mL × 2). The organic extracts were washed with brine and dried over Na_2SO_4. After removal of the solvent, the residue was purified by flash chromatography using toluene/EtOAc (19:1) as eluent to give the corresponding glycosides in 20–60% yield.

General procedure for the deprotection of benzylic groups

A catalytic amount of 10% Pd/C (354.5 mg) was added to a solution of the above-described glycoside (0.207 mmol) in $CHCl_3$ / CH_3OH (2:1, 35 mL). The mixture was stirred for 5 h under a hydrogen atmosphere. The catalyst was filtered off and washed with CH_3OH. The solvent was removed under reduced pressure to afford the deprotected glycoside in 90–95% yield.

General procedure for the preparation of anhydrides

The deprotected glycoside (0.11 mmol) was dissolved in 2 N aqueous KOH (3.73 mmol). After 1 h, the solution was poured into ice/water and acidified with 2 N HCl (3.7 mL). The mixture was extracted with EtOAc/methyl ethyl ketone (9:1), and the organic extracts washed with brine (15%), dried over Na_2SO_4, and concentrated under reduced pressure to give the corresponding anhydride in 80–90% yield.

General procedure for formation of the imide

A solution of the anhydride (0.095 mmol) in anhydrous DMSO (1 mL) and 2-hydrazino-1,3-propanediol (40.6 mg, 0.38 mmol) was stirred at room temperature for 1 h. After removal of the solvent under reduced pressure, the residue was dissolved in water and purified by reversed-phase chromatography (LiChroprep RP-18, 40–63 μm) eluting with H_2O/CH_3CN, 9:1 (30 mL × 3), then 7:3. Fractions containing the product were collected, concentrated, and lyophilized to afford the final glycoside in 75–85% yield.

5*H*-Indolo[2,3-*a*]pyrrolo[3,4-*c*]carbazole-5,7(6*H*)-dione, 12-[2′,6′-dideoxy-4′-*O*-(2″,6″-dideoxy-α-L-galactopyranosyl)-β-L-galactopyranosyl]-12,13-dihydro-2,10-dihydroxy-6-{[2-hydroxy-1-(hydroxymethyl)-ethyl]amino}(**1**). Yellow lyophile, 30% yield from [37]. ^{1}H NMR (300 MHz, [D$_6$]DMSO): δ = 11.20 (s, 1H), 9.80 (br, 2H), 8.89 (d, 1H), 8.87 (d, 1H), 7.38 (s, 1H), 7.06 (s, 1H), 6.80 (m, 2H), 6.30 (m, 1H), 5.56 (s, 1H), 5.06 (s, 1H), 4.78 (s, 1H), 4.54 (m, 2H), 4.28 (m, 2H), 4.13 (m, 2H), 3.80 (s, 1H), 3.50–3.45 (m, 8H), 2.27 (s, 1H), 1.98 (m, 2H), 1.60 (s, 1H), 1.40 (d, 3H), 1.12 ppm (d, 3H); ^{13}C NMR (75 MHz, [D$_6$]DMSO): δ = 169.5, 169.4, 158.6, 158.3, 143.2, 142.5, 128.7, 128.2, 125.9, 118.4, 118.2, 116.3, 115.2, 114.5, 111.2, 111.1, 99.8, 99.3, 97.5, 82.8, 77.3, 74.3, 70.9, 68.2, 67.6, 65.4, 63.2, 61.1, 34.3, 33.1, 23.1, 17.9, 17.6 ppm; HPLC purity: 96.2%, t_R = 7.08 min.

5*H*-Indolo[2,3-*a*]pyrrolo[3,4-*c*]carbazole-5,7(6*H*)-dione, 12-[2′,6′-dideoxy-3′-*O*-(2″,6″-dideoxy-α-L-galactopyranosyl)-β-L-galactopyranosyl]-12,13-dihydro-2,10-dihydroxy-6-{[2-hydroxy-1-(hydroxymethyl)-ethyl]amino}(**2**). Yellow lyophile, 15% yield from [37]. ^{1}H NMR (300 MHz, [D$_6$]DMSO): δ = 11.20 (s, 1H), 9.80 (br, 2H), 8.87 (d, 1H), 8.84 (d, 1H), 7.25 (s, 1H), 7.00 (s, 1H), 6.78 (m, 2H), 6.50 (d, 1H), 6.30 (d, 1H), 5.58 (s, 1H), 5.08 (s, 1H), 4.53 (m, 2H), 4.42 (d, 1H), 4.25 (d, 1H), 4.18 (m, 2H), 4.10 (s, 1H), 3.60 (m, 3H), 3.50–3.30 (m, 8H), 1.80–1.50 (m, 1H), 1.30 (d, 3H), 1.00 ppm (d, 3H); ^{13}C NMR (75 MHz, [D$_6$]DMSO): δ = 169.7, 169.3, 158.4, 158.2, 143.6, 142.2, 128.3, 128.0, 125.2, 118.0, 117.5, 116.1, 115.0, 114.8, 114.2, 111.6, 111.1, 99.2, 99.0, 97.3, 82.5, 77.7, 74.1, 71.2, 68.5, 67.4, 65.2, 63.1, 61.6, 34.2, 33.0, 23.4, 17.4, 17.3 ppm; HPLC purity: 98.5%, t_R = 13.58 min.

5*H*-Indolo[2,3-*a*]pyrrolo[3,4-*c*]carbazole-5,7(6*H*)-dione, 12-[2′,6′-dideoxy-4′-*O*-(2″,6″-dideoxy-α-L-galactopyranosyl)-β-L-glucopyranosyl]-12,13-dihydro-2,10-dihydroxy-6-{[2-hydroxy-1-(hydroxymethyl)-ethyl]amino}(**3**). Yellow lyophile, 25% yield from [37]. ^{1}H NMR (300 MHz, [D$_6$]DMSO): δ = 11.20 (s, 1H), 9.78 (br, 2H), 8.88 (d, 1H), 8.86 (d, 1H), 7.30 (s, 1H), 7.09 (s, 1H), 6.80 (m, 2H), 6.40 (d, 1H), 5.55 (s, 1H), 5.45 (s, 1H), 5.20 (s, 1H), 4.55 (m, 3H), 4.30 (d, 1H), 4.10 (m, 1H), 3.90 (m, 2H), 3.80 (m, 1H), 3.50 (m, 8H), 2.30 (m, 1H), 1.80 (m, 1H), 1.75 (m, 1H), 1.40 (d, 3H), 1.20 ppm (d, 3H); ^{13}C NMR (75 MHz, [D$_6$]DMSO): δ = 169.3, 158.4, 157.9, 143.4, 142.1, 135.8, 128.2, 125.9, 118.6, 118.1, 116.2, 115.4, 114.3, 111.2, 99.7, 99.0, 97.4, 82.5, 81.8, 73.6, 72.3, 71.4, 70.8, 68.0, 67.3, 65.3, 63.0, 60.9, 38.5, 33.0, 22.7, 19.1, 17.6 ppm; HPLC purity: 96.3%, t_R = 14.54 min.

5*H*-Indolo[2,3-*a*]pyrrolo[3,4-*c*]carbazole-5,7(6*H*)-dione, 12-[2′,6′-dideoxy-3′-*O*-(α-L-galactopyranosyl)-β-L-glucopyranosyl]-12,13-dihydro-2,10-dihydroxy-6-{[2-hydroxy-1-(hydroxymethyl)ethyl]amino}(**4**). Orange lyophile, 13% yield from [37]. ^{1}H NMR (300 MHz, [D$_6$]DMSO): δ = 11.20 (s, 1H), 9.78 (br, 2H), 8.88 (d, 1H), 8.86 (d, 1H), 7.30 (s, 1H), 7.09 (s, 1H), 6.80 (m, 2H), 6.50 (d, 1H), 5.50 (m, 2H), 5.15 (d, 1H), 5.10 (d, 1H), 4.80 (d, 1H), 4.50 (t, 2H), 4.30 (br s, 1H), 4.15–4.10 (m, 2H), 3.90 (m, 1H), 3.80 (m, 1H), 3.75 (m, 1H), 3.50 (m, 8H), 3.25–3.20 (m, 2H), 3.10 (m, 1H), 2.30–2.10 (m, 1H), 1.40 ppm (d, 3H); ^{13}C NMR (75 MHz, [D$_6$]DMSO): δ = 169.3, 157.9, 149.6, 142.4, 142.1, 130.0, 125.8, 116.3, 115.4, 114.6, 114.3, 113.5, 111.6, 111.2, 102.1, 98.8, 95.5, 82.4, 82.1, 80.4, 78.5, 77.7, 75.6, 75.2, 74.6, 72.2, 68.5, 63.0, 62.8, 60.9, 22.8, 22.7, 18.8 ppm; HPLC purity: 96.0%, t_R = 12.46 min.

5*H*-Indolo[2,3-*a*]pyrrolo[3,4-*c*]carbazole-5,7(6*H*)-dione, 12-[3′-*O*-(α-L-galactopyranosyl)-β-L-galactopyranosyl]-12,13-dihydro-2,10-dihydroxy-6-{[2-hydroxy-1-(hydroxymethyl)ethyl]amino}(**5**). Orange lyophile, 17% yield from [37]. ^{1}H NMR (400 MHz, [D$_6$]DMSO): δ = 11.60 (s, 1H), 9.90 (br s, 1H), 8.90 (d, 1H), 8.80 (d, 1H), 7.25 (s, 1H), 7.0 (s, 1H), 6.85 (dd, 2H), 6.07 (br s, 1H), 6.01 (d, 1H), 5.56 (d, 1H), 5.13 (br s, 1H), 5.00 (d, 1H), 4.90 (br s, 1H), 4.60 (m, 4H), 4.40 (m, 3H), 4.27–4.12 (m, 2H), 4.00–3.85 (m, 2H), 3.80–3.20 ppm (m, 13H); ^{13}C NMR (75 MHz, [D$_6$]DMSO): δ = 169.7, 169.6, 158.4, 158.3, 144.5, 143.2, 129.1, 127.8, 126.0, 125.8, 118.7, 117.7, 116.4, 114.7, 114.3, 114.2, 111.0, 110.8, 97.8, 97.6, 97.2, 85.2, 80.3, 78.6, 71.4, 70.3, 69.9, 69.3, 66.5, 63.1, 61.1, 60.6 ppm; HPLC purity: 95.5%, t_R = 6.55 min.

5*H*-indolo[2,3-*a*]pyrrolo[3,4-*c*]carbazole-5,7(6*H*)-dione, 12-[3′-*O*-(α-D-glucopyranosyl)-β-L-galactopyranosyl]-12,13-dihydro-2,10-dihydroxy-6-{[2-hydroxy-1-(hydroxymethyl)ethyl]amino}(**6**). Orange lyophile, 36% yield from [37]. ^{1}H NMR (400 MHz, [D$_6$]DMSO): δ = 11.65 (s, 1H), 9.90 (br s, 1H), 8.90 (d, 1H), 8.80 (d, 1H), 7.23 (s, 1H), 7.00

(s, 1H), 6.87 (dd, 2H), 6.01 (d, 1H), 5.57 (d, 1H), 5.30 (br s, 1H), 5.10 (d, 1H), 4.95 (m, 3H), 4.77 (d, 1H), 4.57 (m, 2H), 4.48–4.23 (m, 3H), 4.15 (t, 1H), 3.96 (dd, 1H), 3.86–3.60 (m, 5H), 3.60–3.44 (m, 9H), 3.17 (m, 1H), 3.08 ppm (m, 1H); ^{13}C NMR (75 MHz, [D$_6$]DMSO): $\delta =$ 170.0, 169.9, 158.6, 158.5, 144.6, 143.5, 129.3, 128.0, 126.1, 118.9, 118.0, 116.6, 115.0, 114.5, 114.4, 111.0, 101.0, 97.7, 97.6, 85.0, 82.4, 79.3, 74.4, 73.8, 73.3, 71.2, 71.0, 70.6, 69.0, 63.3, 61.8, 61.3 ppm; HPLC purity: 92.1%, $t_R = 6.39$ min.

5*H*-Indolo[2,3-*a*]pyrrolo[3,4-*c*]carbazole-5,7(6*H*)-dione, 12-[6′-*O*-(β-D-glucopyranosyl)-β-D-glucopyranosyl]-12,13-dihydro-2,10-dihydroxy-6-{[2-hydroxy-1-(hydroxymethyl)ethyl]amino}(**7**). Pale-orange lyophile, 29% yield from [37]. ^{1}H NMR (300 MHz, [D$_6$]DMSO): $\delta = 11.20$ (s, 1H), 9.76 (br, 2H), 8.90–8.80 (m, 2H), 7.30–7.10 (m, 2H), 6.80 (m, 2H), 6.20 (br s, 1H), 5.80 (d, 1H), 4.30 (d, 1H), 4.25 (d, 1H), 4.20 (m, 1H), 4.15–3.98 (m, 3H), 3.60–3.55 (m, 3H), 3.50–3.30 (m, 11H), 3.25 (m, 3H), 3.0 ppm (m, 2H); ^{13}C NMR (75 MHz, [D$_6$]DMSO): $\delta =$ 169.6, 158.4, 157.5, 145.0, 143.2, 141.8, 130.3, 129.6, 128.4, 125.8, 119.4, 118.9, 116.4, 116.0, 115.8, 115.3, 114.7, 114.4, 111.0, 104.0, 103.5, 98.0, 85.5, 76.7, 77.8, 77.5, 77.4, 77.0, 74.1, 73.4, 70.6, 69.0, 63.2, 61.6, 61.1 ppm; HPLC purity: 98.9%, $t_R = 6.08$ min.

5*H*-Indolo[2,3-*a*]pyrrolo[3,4-*c*]carbazole-5,7(6*H*)-dione, 12-[3′-*O*-(α-D-glucopyranosyl)-β-D-glucopyranosyl]-12,13-dihydro-2,10-dihydroxy-6-{[2-hydroxy-1-(hydroxymethyl)ethyl]amino}(**8**). Pale-orange lyophile, 13% yield from [37]. ^{1}H NMR (300 MHz, [D$_6$]DMSO): $\delta = 11.20$ (s, 1H), 9.76 (br, 2H), 8.86 (d, 1H), 8.84 (d, 1H), 7.25 (s, 1H), 7.01 (s, 1H), 6.85 (m, 2H), 6.25 (d, 1H), 6.15 (br, 1H), 5.55 (m, 2H), 5.2 (br, 1H), 4.98 (s, 1H), 4.85 (br, 1H), 4.75 (br, 1H), 4.55 (br, 3H), 4.20 (m, 2H), 4.00 (m, 2H), 3.75–3.60 (m, 3H), 3.40 (m, 8H), 3.3 (m, 2H), 2.9 ppm (m, 1H); ^{13}C NMR (75 MHz, [D$_6$]DMSO): $\delta =$ 169.8, 169.7, 158.7, 158.6, 145.3, 144.0, 130.3, 128.7, 126.0, 119.9, 118.5, 116.9, 115.2, 115.1, 114.7, 111.3, 111.2, 101.5, 98.5, 98.4, 87.2, 85.1, 78.4, 74.2, 73.4, 73.3, 72.2, 70.7, 68.3, 63.4, 61.3, 61.2, 59.00 ppm; HPLC purity: 96.2%, $t_R = 8.91$ min.

5*H*-Indolo[2,3-*a*]pyrrolo[3,4-*c*]carbazole-5,7(6*H*)-dione, 12-[2′-*O*-(α-D-glucopyranosyl)-β-D-glucopyranosyl]-12,13-dihydro-2,10-dihydroxy-6-{[2-hydroxy-1-(hydroxymethyl)ethyl]amino}(**9**). Pale-yellow lyophile, 32% yield from [37]. ^{1}H NMR (300 MHz, [D$_6$]DMSO): $\delta = 11.11$ (s, 1H), 10.00 (br s, 1H), 9.95 (br s, 1H), 8.87 (d, 1H), 8.80 (d, 1H), 7.28 (s, 1H), 7.00 (s, 1H), 6.85 (m, 1H), 6.83 (m, 1H), 6.26 (d, 1H), 5.95 (br s, 1H), 5.53 (s, 1H), 5.20 (br s, 1H), 4,56 (s, 2H), 4.40 (m, 1H), 4,17 (br s, 1H), 4.01 (m, 2H), 3.86 (m, 1H), 3.76 (m, 2H), 3.50 (m, 4H), 3.35 (m, 4H), 2.87 (m, 2H), 2.47 ppm (m, 2H); ^{13}C NMR (75 MHz, [D$_6$]DMSO): $\delta =$ 169.6, 169.5, 158.9, 158.6, 144.2, 144.0, 130.1, 128.0, 126.2, 125.8, 119.2, 118.4, 116.8, 114.9, 114.9, 114.2, 111.6, 111.0, 99.0, 98.3, 97.4, 83.1, 80.4, 78.7, 76.1, 73.5, 72.9, 71.9, 69.8, 68.1, 63.3, 61.0, 60.4, 58.8 ppm; HPLC purity: 98.7%, $t_R =$ 6.52 min.

5*H*-Indolo[2,3-a]pyrrolo[3,4-c]carbazole-5,7(6*H*)-dione, 12-[3′-O-(α-L-glucopyranosyl)-β-D-glucopyranosyl]-12,13-dihydro-2,10-dihydroxy-6-{[2-hydroxy-1-(hydroxymethyl)ethyl]amino}(**10**). Yellow lyophile, 22% yield from [37]. ^{1}H NMR (300 MHz, [D$_6$]DMSO): $\delta = 11.25$ (s, 1H), 9.80 (br, 2H), 8.85 (d, 1H), 8.83 (d, 1H), 7.25 (s, 1H), 7.01 (s, 1H), 6.85 (m, 2H), 6.10 (d, 1H), 6.10 (br, 1H), 5.60 (m, 1H), 5.10 (m, 2H), 4.90 (s, 1H), 4.70–4.60 (m, 3H), 4.55 (br s, 2H), 4.50 (m, 1H), 4.10 (br, 3H), 3.80 (m, 1H), 3.75–3.60 (m, 4H), 3.65–3.30 (m, 6H), 3.15 (m, 1H), 3.05 ppm (m, 1H); ^{13}C NMR (75 MHz, [D$_6$]DMSO): $\delta =$ 169.6, 169.5, 158.5, 158.3, 145.1, 143.7, 130.1, 128.4, 125.8, 119.7, 118.3, 116.7, 115.0, 114.8, 114.5, 111.0, 110.9, 100.9, 98.2, 98.1, 86.7, 84.4, 78.8, 74.0, 73.4, 73.0, 70.7, 70.4, 66.8, 63.2, 61.3, 61.1, 58.9 ppm; HPLC purity: 94.9%, $t_R = 6.95$ min.

5*H*-Indolo[2,3-*a*]pyrrolo[3,4-*c*]carbazole-5,7(6*H*)-dione, 12-[3′-*O*-(α-D-glucopyranosyl)-α-D-glucopyranosyl]-12,13-dihydro-2,10-dihydroxy-6-{[2-hydroxy-1-(hydroxymethyl)ethyl]amino}(**11**). Yellow lyophile, 33% yield from [37]. ^{1}H NMR (300 MHz, [D$_6$]DMSO): $\delta = 11.50$ (s, 1H), 9.73 (br s, 2H), 8.87 (d, 1H), 8.80 (d, 1H), 6.95 (s, 1H), 6.90 (m, 2H), 6.75 (d, 1H), 6.30 (s, 1H), 6.20 (br s, 1H), 5.60 (br s, 2H), 5.10 (br s, 1H), 4.98 (br s, 2H), 4.80 (br s, 2H), 4.50 (m, 2H), 4.30 (br s, 1H), 4.20 (m, 2H), 4.15 (s, 1H), 4.0 (s, 1H), 3.75 (m, 1H), 3.60 (m, 2H), 3.50 (m, 8H), 3.20 ppm (m, 2H); ^{13}C NMR (75 MHz, [D$_6$]DMSO): $\delta =$ 170.1, 170.0, 158.5, 143.0, 142.8, 130.9, 130.6, 126.4, 126.0, 118.5, 117.9, 116.3, 114.7, 114.3, 114.2, 111.1, 110.4, 100.2, 97.2, 96.5, 82.9, 78.9, 77.7, 74.5, 73.9, 72.7, 70.8, 69.3, 65.0, 63.4, 61.4, 61.3, 58.7 ppm; HPLC purity: 92.4%, $t_R = 7.14$ min.

5*H*-Indolo[2,3-*a*]pyrrolo[3,4-*c*]carbazole-5,7(6*H*)-dione, 12-[3′-*O*-(β-D-glucopyranosyl)-β-D-glucopyranosyl]-12,13-dihydro-2,10-dihydroxy-6-{[2-hydroxy-1-(hydroxymethyl)ethyl]amino}(**12**). Pale-orange lyophile, 29% yield from [37]. ^{1}H NMR (300 MHz, [D$_6$]DMSO): $\delta = 11.20$ (s, 1H), 9.78 (br, 2H), 8.87 (d, 1H), 8.85 (d, 1H), 7.18 (s, 1H), 7.00 (s, 1H), 6.85 (m, 2H), 6.25 (d, 1H), 6.18 (br, 1H), 5.6 (m, 1H), 5.1 (m, 4H), 4.75 (m, 1H), 4.65 (br, 1H), 4.55 (m, 2H), 4.3 (d, 1H), 4.1–3.9 (m, 3H), 3.8 (br, 1H), 3.75–3.65 (m, 3H), 3.55–3.35 (m, 6H), 3.29 (m, 1H), 3.25 (m, 1H), 3.25 (m, 1H), 3.20 (m, 1H), 3.1 (m, 1H), 2.9 ppm (m, 1H); ^{13}C NMR (75 MHz, [D$_6$]DMSO): $\delta =$ 169.8, 169.7, 158.5, 158.4, 144.8, 143.6, 129.0, 129.6, 128.2, 126.6, 118.5, 118.3, 116.4, 115.2, 114.5, 114.1, 111.3, 101.6, 98.5, 97.4, 84.2, 82.5, 79.3, 75.4, 73.9, 73.2, 71.5, 71.2, 71.0, 70.4, 69.3, 63.2, 61.5, 61.1 ppm; HPLC purity: 93.7%, $t_R = 8.84$ min.

5*H*-Indolo[2,3-*a*]pyrrolo[3,4-*c*]carbazole-5,7(6*H*)-dione, 12-[3′-*O*-(β-L-glucopyranosyl)-β-D-glucopyranosyl]-12,13-dihydro-2,10-dihydroxy-6-{[2-hydroxy-1-(hydroxymethyl)ethyl]amino}(**13**). Yellow lyophile, 32% yield from [37]. ^{1}H NMR (300 MHz, [D$_6$]DMSO): $\delta = 11.20$ (s, 1H), 9.75 (br, 2H), 8.86 (d, 1H), 8.84 (d, 1H), 7.20 (s, 1H), 6.85 (s, 1H), 6.80 (m, 2H), 6.10 (d, 1H), 5.85 (br s, 1H), 5.60 (s, 1H), 5.56 (br s, 1H), 5.30 (br s, 1H), 4.80 (m, 1H), 4.60 (m, 2H), 4.30 (m, 2H), 4.15 (m, 1H), 4.10 (m, 3H), 3.75 (m, 3H), 3.50–3.55 (m, 7H), 3.20 (m, 3H), 2.80 ppm (m, 2H); ^{13}C NMR (75 MHz, [D$_6$]DMSO): $\delta =$ 169.5, 169.4, 158.5, 158.3, 145.0, 143.8, 130.0, 128.3, 125.9, 119.5, 118.3, 116.7, 115.0, 114.8, 114.5, 111.1, 111.0, 104.7, 98.2, 98.0, 88.2, 84.3, 78.0, 77.4, 76.5, 74.4, 72.2, 70.5, 67.0, 63.2, 61.4, 61.1, 58.8 ppm; HPLC purity: 96.6%, $t_R = 9.02$ min.

Biology

Cell cultures. Human carcinoma cell lines A2780 (ovary), H460 (lung), and GLC4 (small-cell lung) were maintained in RPMI 1640 (Gibco/BRL) supplemented with fetal calf serum (10%), glutamine (2 mM), penicillin (100 U), and streptomycin (100 μg) at 37 °C in a humidified incubator (5% CO_2, 95% air).

Cytotoxicity assay. The cytotoxicity of the new indolocarbazole derivatives was determined using the sulforhodamine B (SRB) assay.[49] All compounds were dissolved in sterile DMSO and diluted in saline (0.9% NaCl) immediately before use. A2780 (2000 cells/well), H460 (1500 cells/well), and GLC4 (1500 cells/well) cell lines were seeded in 96-well microtiter plates and incubated for 24 h at 37 °C in a 5% CO_2 incubator. Drugs were then added to the wells to achieve final drug concentrations in the range of 0.001–10 μM. After drug exposure for 24 h, cells were washed twice with phosphate buffered-saline (PBS) and incubated in a drug-free medium for about three doubling times (72 h), and the cellular viability was then measured by the SRB assay. IC_{50} values (the concentration achieving 50% cellular mortality relative to untreated control) were

evaluated by a curve in which the surviving percentage of cells is plotted as a function of the drug concentration.

Evaluation of antitumor activity. Human tumor cell lines A2780 (ECACC) were prepared by subcutaneous (s.c.) in vivo injection of tumor cells (10×10^6 cells/flank/0.2 mL). Tumor cells were suspended in a sterile solution of NaCl (0.9%) and 0.2 mL of this suspension was injected into the right flank of female nude mice. Female athymic nude mice, 6–8 weeks old, were purchased from Harlan Italy, maintained in microisolator cages, and supplied with sterile materials under standard conditions according to UKCCCR guidelines.[50] Tumor growth was followed by caliber measurement of length and width at predetermined times (weekly or twice weekly). Tumor volume (TV in mm^3) was calculated using the formula: $TV = width^2\times(length/2)$.[51] All compounds were dissolved in sterile water for injection and diluted in saline (0.9% NaCl) immediately before use. Compounds were administered i.v. at different schedules and dosages as indicated in the single experiments at a dose volume of 10 mL kg^{-1}. Drug treatments started when tumors were approximately 50 mm^3 in volume.

The following effects achieved by the drug treatment were evaluated: percent tumor volume inhibition (TVI%) in treated versus control mice, determined at the nadir of tumor volume in the treated group; log cell kill (LCK) in treated mice according to the formula: $T-C/DT\times3.32$, for which T and C represent the time (in days) taken by the tumors in treated (T) and control (C) mice to reach a predetermined volume, specified in each experiment.[52] DT is the tumor doubling time calculated from semilogarithmic best-fit curve of tumor volume in the control group, plotted versus time, when the growth of tumor was in the exponential phase. Toxic deaths are the number of dead mice showing no measurable tumor mass or mice dead before the first death of the control group.

Topoisomerase I cleavage assay. Recombinant human top1 was purified from a yeast strain.[53] The purified isozyme was stored at −80 °C in 500 mM Tris-HCl, pH 7.7, 200 mM KCl, 10 mM EDTA, 10 mM EGTA, and 10% glycerol. SV40 DNA was linearized with EcoRI and labeled with α-[^{32}P]dATP in the presence of the Klenow fragment of DNA polymerase I. The labeled DNA was then digested to completion with BamHI to generate uniquely 3′-end-labeled fragments, which were separated by agarose gel electrophoresis and purified by ion-exchange chromatography (QIAGEN). DNA cleavage levels in top1 DNA cleavage reactions were performed in a volume of 20 μL in 20 mM Tris-HCl, pH 7.5, 50 mM KCl, 0.5 mM dithiothreitol (DTT), 0.5 mM EDTA for 20 min at 37 °C. Reactions were stopped by adding SDS and proteinase K (0.1% and 0.1 mg mL^{-1} final concentrations, respectively) and further incubated at 45 °C for 20 min. After precipitation with EtOH, the samples were resuspended in 2.5 μL formamide–TBE loading buffer, 0.1% xylene cyanol, and 0.1% bromophenol blue, heated to 95 °C for 2 min, chilled on ice, and then loaded onto an 8% polyacrylamide denaturing sequencing gel (7 M urea, 89 mM Tris-HCl, pH 8.0, 89 mM boric acid, 2 mM EDTA). Gels were run at 70 W for 2 h. Autoradiograms of dried gels were carried out by using Amersham Hyperfilm.

NMR studies

^{1}H NMR experiments were performed on a Varian 300 MHz spectrometer and processed using Xwin-NMR version 2.1. For assignment of the spin systems, TOCSY (total correlation spectroscopy)[54] and NOESY (nuclear Overhauser enhanced spectroscopy)[44] spectra were recorded in the phase-sensitive mode using TPPI (time-proportional phase increments method) for compounds **1** and **2**. NOESY spectra were collected at 300 K with mixing times varying from 100 to 200 ms. No evidence of spin diffusion was observed up to a mixing time of 200 ms. The spectral width was 6400 Hz in both dimensions, with 4 K points in *t*2 and 256 data points in *t*1 and 96 scans at each increment. Forward linear prediction to 512 points and zero filling to 1024 were applied to the incremented dimension. Sinusoidal apodisation was used in both *t*2 and *t*1. Cross-peak intensities from the 200 ms spectrum were classified in three different categories: s (strong), m (medium), w (weak).

Molecular Modeling

Software and general methods. Ab initio calculations were performed with Gaussian 98.[55] AMBER package version 5[56] was used for molecular mechanics geometry optimizations and molecular dynamics simulations. These calculations were carried out with GLYCAM_93,[46] an extension of the AMBER force field[45] to carbohydrates. The parameters added (Supporting Information) to GLYCAM_93 force field to improve the description of the indolocarbazoles and the non-standard residue phosphotyrosine (P-Tyr723) in the covalent top1–DNA complex were calculated ab initio, or assigned by analogy with existing parameters. Partial charges for indolocarbazoles and P-Tyr723 (Supporting Information) were derived from ab initio molecular electrostatic potential calculated at HF/6-31G*//HF/3-21G(*) level. Electrostatic potential fitting was performed using the RESP program.[57] MD simulations of ligands and complexes had the following characteristics: the NPT ensemble and the coupling with a Berendsen thermal bath[58] were employed; distance-dependent ($\varepsilon=4r$) and constant ($\varepsilon=1$) dielectric constants were used respectively for MD simulations in vacuo and in solution; the time step was 2 fs and the SHAKE algorithm[59] was applied; gradual heating from 0 to 298 K was performed over 60 ps, molecules were then equilibrated for 40 ps, data collection periods were specified for each calculation. Structures obtained from the sampling of MD trajectories were clustered at RMS thresholds of 0.5 Å for distances and 5° for dihedral angles using the program FRAMES.[60] Solvent-accessible surface and buried surface of the ligand were determined applying the Connolly algorithm.[61,62] GOLD[49] was employed with default settings to obtain 50 poses for each docked molecule; the score was calculated using the GoldScore fitness function.

Isolated ligands. The crystal structure of rebeccamycin (CSD code: DETDIP)[63] was used as reference to test the ability of quantum mechanical and molecular mechanics methods in predicting the geometry of indolocarbazoles. The X-ray structure was optimized using ab initio calculations at HF/3-21G(*) level of theory, and the RMSD between crystal and computed geometries was 0.18 Å. The improved GLYCAM_93 force field was then employed to minimize the energy of rebeccamycin, and the RMSD between ab initio and molecular mechanics coordinates was 0.17 Å. The ability of the force field in predicting geometries of indolocarbazoles was further established considering edotecarin. In this case the RMSD between coordinates obtained from HF/3-21G(*) calculation and the improved GLYCAM_93 force field was 0.26 Å.

MD simulations in aqueous solution of **1** and **2** were carried out by soaking the ligand in a box of TIP3p[64] water molecules and applying Periodic Boundary Conditions.[65] The general MD protocol described above was used with an additional period of 15 ps, needed to equilibrate the water box at constant pressure. van der Waals and electrostatic intermolecular interactions were treated with the standard procedure and with Particle Mesh Ewald,[66,67] which im-

plied a summation over the reciprocal space and was physically more correct. In the data collection period of 2 ns, trajectories were sampled every 2 ps. The average potential energies during simulations were calculated for iso1 and iso2 (Figure 5) conformations of **1** and **2**. With the standard procedure, **1** (iso1) is 2.4 kcal mol^{-1} more stable than **1** (iso2), while **2** (iso1) is 11.7 kcal mol^{-1} higher in energy than **2** (iso2). Using Particle Mesh Ewald iso1 is the most stable conformation for both indolocarbazoles; the energy differences of iso2 are 0.5 and 6.3 kcal mol^{-1} for **1** and **2**, respectively.

Ternary complexes. The X-ray structure (PDB code: 1A31) of the top1–DNA cleavable complex was modified by removing water molecules, converting the iodouracil residues into thymines, and the T–A base pair in position +1 into a G–C base pair.[26] After addition of hydrogen atoms, the geometry of the complex was refined with 1000 steps of conjugate gradient energy minimization. The target region for the MD docking of **1** into the top1–DNA cleavable complex was defined by five residues, namely G+1s, C+1i, Arg 364, Asp 533, and Asn 722, selected on the basis of literature findings.[26] The geometric center (P) of target residues was set as the center of a sphere of radius 30 Å, and on its surface 100 random points were generated according to the von Neumann–Marsaglia algorithm.[68,69] Each point defines a potential direction of approach for the ligand to the target region of the biomolecular system. Four starting points were chosen by visual inspection to drive the ligand through paths with small steric hindrance. The center of mass of **1** (iso1) and **1** (iso2) were positioned on each point, obtaining eight starting geometries for dynamic docking. MD simulations were carried out with the standard protocol. For the duration of the heating period, a distance constraint was imposed along the P-ligand vector to bring **1** closer to the target region. All top1–DNA complex residues with at least one atom within 15 Å of P were allowed to move during the simulation. In the equilibration and data collection (60 ps) phases, the constraint was released and the trajectories were sampled every 0.2 ps. The structures of top1–DNA–ligand complexes obtained for each simulation were clustered using nine distances between three fixed points (not involved in MD) of the biomolecules, three points of the aglycone of **1**, and the three dihedral angles of the glycosidic bonds of **1**, thus collecting thirty representative conformations. These structures were geometry optimized to a gradient of 0.01 kcal mol^{-1} Å^{-1}, and this process involved only **1** and residues that were free to move in the course of MD. The most stable top1–DNA–**1** complex in which **1** exhibits an iso1 conformation was selected to be used as a model. The structures of the ternary complexes for five different indolocarbazoles (**2**, **4**, **8**, **9**, and **12**) were then built by attaching the relevant disaccharide, in an iso1 conformation, to the aglycone of the model. The top1–DNA–indolocarbazole complexes were submitted to MD simulations with standard protocol and 1 ns of data collection time. The resulting trajectories were sampled every picosecond, and the conformers were clustered as described above. A total of eight representative structures were obtained, one for the complexes of **1**, **4**, **9**, and **12**, and two for **2** and **8**. Solvent-accessible surface and buried surface (Tables 3 and 4) of the ligands were evaluated on the eight representative structures. The average intermolecular distances (Supporting Information) between indolocarbazoles and biomolecules were measured over the whole data collection time of the MD.

The GOLD program was employed to dock **1**, **2**, **4**, **8**, **9**, **12**, and SA315F into the top1–DNA binary complex extracted from the X-ray structure (PDB code: 1SEU) of the top1–DNA–SA315F ternary complex.[27] The active site origin was defined in the same way as the center of the target region of the MD defined above, and the active site radius was 15 Å.

Acknowledgements

The work was supported by Istituto Mobiliare Italiano (Grant no. 66165). We thank A. Giolitti for helpful discussions in molecular modeling studies, A. Cartoni and A. Ettorre for analytical assistance, and D. Fattori for previewing the manuscript.

Keywords: antitumor agents · disaccharides · indolocarbazole glycosides · topoisomerase inhibitors

[1] U. Pindur, Y.-S. Kim, F. Mehrabani, *Curr. Med. Chem.* **1999**, *6*, 29–69.
[2] J. C. Wang, *Annu. Rev. Biochem.* **1996**, *65*, 635–692.
[3] J. J. Champoux, *Annu. Rev. Biochem.* **2001**, *70*, 369–413.
[4] L. Stewart, M. R. Redinbo, X. Qiu, W. G. J. Hol, J. J. Champoux, *Science* **1998**, *279*, 1534–1541.
[5] M. R. Redinbo, J. J. Champoux, W. G. J. Hol, *Biochemistry* **2000**, *39*, 6832–6840.
[6] C. Bailly, J.-F. Riou, P. Colson, C. Houssier, E. Rodrigues-Pereira, M. Prudhomme, *Biochemistry* **1997**, *36*, 3917–3929.
[7] G. Zhang, J. Shen, H. Cheng, L. Zhu, L. Fang, S. Luo, M. Muller, G. E. Lee, L. Wei, Y. Du, D. Sun, P. G. Wang, *J. Med. Chem.* **2005**, *48*, 2600–2611.
[8] J. Wang, N. Soundarajan, N. Liu, K. Zimmermann, B. N. Naidu, *Tetrahedron Lett.* **2005**, *46*, 907–910.
[9] F. Anizon, P. Moreau, M. Sancelme, W. Laine, C. Bailly, M. Prudhomme, *Bioorg. Med. Chem.* **2003**, *11*, 3709–3722.
[10] C. Marminon, A. Pierrè, B. Pfeiffer, V. Perez, S. Leonce, P. Renard, M. Prudhomme, *Bioorg. Med. Chem.* **2003**, *11*, 679–687.
[11] C. Marminon, M. Facomprè, C. Bailly, J. Hickman, A. Pierrè, B. Pfeiffer, P. Renard, M. Prudhomme, *Eur. J. Med. Chem.* **2002**, *37*, 435–440.
[12] A. Voldoire, M. Sancelme, M. Prudhomme, P. Colson, C. Housiier, C. Bailly, S. Leonce, S. Lambel, *Bioorg. Med. Chem.* **2001**, *9*, 357–365.
[13] P. Moreau, M. Sancelme, C. Bailly, S. Leonce, A. Pierrè, J. Hickman, B. Pfeiffer, M. Prudhomme, *Eur. J. Med. Chem.* **2001**, *36*, 887–897.
[14] M. Ohkubo, T. Nishimura, H. Kawamoto, M. Nakano, T. Honma, T. Yoshinari, H. Arakawa, H. Suda, H. Orishima, S. Nishimura, *Bioorg. Med. Chem. Lett.* **2000**, *10*, 419–422.
[15] W. A. Denny, *IDrugs* **2004**, *7*, 173–177.
[16] M. G. Saulnier, B. N. Balasubramanian, B. H. Long, et al., *J. Med. Chem.* **2005**, *48*, 2258–2261.
[17] M. Prudhomme, *Curr. Med. Chem. Anticancer Agents* **2004**, *4*, 509–521.
[18] M. Prudhomme, *Eur. J. Med. Chem.* **2003**, *38*, 123–140.
[19] M. Prudhomme, *Curr. Med. Chem.* **2000**, *7*, 1189–1212.
[20] C. Bailly, X. Qu, F. Anizon, M. Prudhomme, J.-F. Riou, J. B. Chaires, *Mol. Pharmacol.* **1999**, *55*, 377–385.
[21] P. Moreau, F. Anizon, M. Sancelme, M. Prudhomme, C. Bailly, D. Severe, J.-F. Riou, D. Fabbro, T. Meyer, A.-M. Aubertin, *J. Med. Chem.* **1999**, *42*, 584–592.
[22] A. Cipollone, M. Berettoni, M. Bigioni, M. Binaschi, C. Cermele, E. Monteagudo, L. Olivieri, D. Palomba, F. Animati, C. Goso, C. A. Maggi, *Bioorg. Med. Chem.* **2002**, *10*, 1459–1470.
[23] M. Facompre, C. Carrasco, P. Colson, C. Houssier, J. D. Chisholm, D. L. Van Vranken, C. Bailly, *Mol. Pharmacol.* **2002**, *62*, 1215–1227.
[24] C. Carrasco, M. Facompre, J. D. Chisholm, D. L. Van Vranken, W. D. Wilson, C. Bailly, *Nucleic Acids Res.* **2002**, *30*, 1774–1781.
[25] X. Qu, J. B. Chaires, M. Ohkubo, T. Yoshinari, S. Nishimura, C. A. Bailly, *Anticancer Drug Des.* **1999**, *14*, 433–442.
[26] M. R. Redinbo, L. Stewart, P. Kuhn, J. J. Champoux, W. G. J. Hol, *Science* **1998**, *279*, 1504–1513.
[27] B. L. Staker, M. D. Feese, M. Cushman, Y. Pommier, D. Zembower, L. Stewart, A. B. Burgin, *J. Med. Chem.* **2005**, *48*, 2336–2345.
[28] K. C. Nicolaou, S. P. Seitz, D. P. Papahatjis, *J. Am. Chem. Soc.* **1983**, *105*, 2430–2434.
[29] V. Bolitt, C. Mioskowski, *J. Org. Chem.* **1990**, *55*, 5812–5813.
[30] B. Iselin, T. Reichstein, *Helv. Chim. Acta* **1944**, *27*, 1200–1203.

[31] B. Classon, P. J. Garegg, B. Samuelsson, *Acta Chem. Scand. Ser. B* **1984**, *38*, 419–422.
[32] S. Nambiar, J. F. Daeubl, R. J. Doyle, K. Grant Taylor, *Tetrahedron Lett.* **1989**, *30*, 2179–2182.
[33] D. Horton, W. Priebe, M. Sznaidman, *Carbohydr. Res.* **1990**, *205*, 71–86.
[34] R. U. Lemieux, A. R. Morgan, *Can. J. Chem.* **1965**, *43*, 2190–2198.
[35] G. H. Veeneman, J. H. van Boom, *Tetrahedron Lett.* **1990**, *31*, 275–278.
[36] P. Smid, G. A. de Ruiter, G. A. van der Marel, F. M. Rombouts, J. H. van Boom, *J. Carbohydr. Chem.* **1991**, *10*, 833–849.
[37] N. Najima, R. Abe, O. Yonemitsu, *Chem. Pharm. Bull.* **1988**, *36*, 4244–4247.
[38] R. Gigg, C. D. Warren, *J. Chem. Soc. C* **1968**, 1903–1911.
[39] N. Adams, C. Blake, M. J. Broadhurst, D. J. Bushnell, C. H. Hassall, H. R. Hartmann, E. Keech, A. R. Stratton, G. J. Thomas, *J. Med. Chem.* **1990**, *33*, 2375–2379.
[40] Z. Zhang, G. Magnusson, *J. Org. Chem.* **1995**, *60*, 7304–7315.
[41] M. Ohkubo, H. Kawamoto, T. Ohno, M. Nakano, H. Morishima, *Tetrahedron* **1997**, *53*, 585–592.
[42] M. Ohkubo, S. Nishimura, H. Jona, T. Honma, H. Morishima, *Tetrahedron* **1996**, *52*, 8099–8112.
[43] K. Kojiri, H. Kondo, H. Arakawa, M. Ohkubo, H. Suda, US Patent 5,804,564, **1998**.
[44] A. Bax, D. G. Davis, *J. Magn. Reson.* **1965**, *63*, 355–360.
[45] W. D. Cornell, P. Cieplak, C. I. Bayly, I. R. Gould, K. M. Merz, D. M. Ferguson, D. C. Spellmeyer, T. Fox, J. W. Caldwell, P. A. Kollman, *J. Am. Chem. Soc.* **1995**, *117*, 5179–5197.
[46] R. J. Woods, R. A. Dwek, C. J. Edge, B. Fraser-Reid, *J. Phys. Chem.* **1995**, *99*, 3832–3846.
[47] C. Bailly, C. Carrasco, F. Hamy, H. Vezin, M. Prudhomme, A. Saleem, E. Rubin, *Biochemistry* **1999**, *38*, 8605–8611.
[48] G. Jones, P. Willett, R. C. Glen, A. R. Leach, R. Taylor, *J. Mol. Biol.* **1997**, *267*, 727–748.
[49] P. Skehan, R. Storeng, D. Scudiero, A. Monks, J. McMahon, D. Vistica, J. T. Warren, H. Bokesh, S. Kenney, M. R. Boyd, *J. Natl. Cancer Inst.* **1990**, *82*, 1107–1112.
[50] *United Kingdom Co-ordinating Committee on Cancer Research (UKCCCR) Guidelines for the Welfare of Animals in Experimental Neoplasia*, 2nd ed., *Br. J. Cancer* **1998**, *77*, 1 – 10.
[51] "Protocols for screening chemical agents and natural products against animal tumors and other biological systems": R. I. Geran, N. H. Greenberg, M. M. MacDonald, A. M. Schumacher, B. J. Abbott, *Cancer Chemother. Rep.* **1972**, *3*, 1–88.
[52] B. A. Teicher, *Anticancer Drug Development Guide. Preclinical screening, clinical trials, and approval*, Humana, Totowa, NJ (USA), **1997**.
[53] G. L. Beretta, M. Binaschi, E. Zagni, L. Capuani, G. Capranico, *Cancer Res.* **1999**, *59*, 3689–3697.
[54] S. Macura, Y. Huang, D. Suter, R. Ernst, *J. Magn. Reson.* **1981**, *43*, 259–281.
[55] M. J. Frisch et al., Gaussian 98, revision A.7; Gaussian, Inc.; Pittsburgh, PA (USA), **1998**.
[56] D. A. Pearlman, D. A. Case, J. W. Caldwell, W. S. Ross, T. E. Cheatham III, S. DeBolt, D. C. Ferguson, G. Seibel, P. A. Kollman, *Comp. Phys. Commun.* **1995**, *91*, 1–41.
[57] C. I. Bayly, P. Cieplak, W. D Cornell, P. A. Kollman, *J. Phys. Chem.* **1993**, *97*, 10269–10280.
[58] H. J. C. Berendsen, J. P. M. Postma, W. F. van Gusteren, A. Di Nola, J. R. Haak, *J. Chem. Phys.* **1984**, *81*, 3684–3690.
[59] J. P. Ryckaert, G. Ciccotti, H. J. C. Berendsen, *J. Comput. Phys.* **1977**, *23*, 327–341.
[60] R. Boggia, M. Fanciullo, L. Finzi, O. Incani, L. Mosti, *Farmaco* **1999**, *54*, 202–212.
[61] M. L. Connolly, *Science* **1983**, *221*, 709–713.
[62] M. L. Connolly, *J. Appl. Crystallogr.* **1983**, *16*, 548–558.
[63] F. H. Allen, *Acta Crystallogr. Sect. B* **2002**, *58*, 380–388.
[64] W. L. Jorgensen, J. Chandrasekhar, J. D. Madura, R. W. Impey, M. L. Klein, *J. Chem. Phys.* **1983**, *79*, 926–935.
[65] J. A. McCammon, S. C. Harvey, *Dynamics of Protein and Nucleic Acids*, Cambridge University Press, Cambridge (UK), **1987**.
[66] P. P. Ewald, *Ann. Phys.* **1921**, *369*, 253–287.
[67] Z.-M. Chen, T. Çağin, W. A. Goddard III, *J. Comput. Chem.* **1997**, *18*, 1365–1370.
[68] "Various Techniques Used in Connection with Random Digits": J. von Neumann, *NBS Appl. Math. Ser.* **1951**, *12*, 36 – 38. Washington, DC: U.S. Government Printing Office.
[69] G. Marsaglia, *Ann. Math. Stat.* **1972**, *43*, 645–646.

Received: August 31, 2007
Revised: October 4, 2007
Published online on December 21, 2007

